# Salt-freshwater dynamics in a subterranean estuary over a spring-neap tidal cycle

C. Robinson,[1] B. Gibbes,[1] H. Carey,[1] and L. Li[1,2]

Received 13 August 2006; revised 30 March 2007; accepted 4 June 2007; published 13 September 2007.

[1] This paper presents field measurements and numerical simulations of pore water salinities and groundwater flow in the intertidal zone of an unconfined coastal aquifer over a spring-neap tidal cycle. The study provides insight into the extent and time-scales of mixing between fresh groundwater and recirculating seawater in a tidally influenced subterranean estuary. Salt-freshwater dynamics in subterranean estuaries are currently not well understood despite their potentially important implications for fluxes of chemicals to coastal waters via submarine groundwater discharge. The data and simulation results show that changes in the tidal shoreline excursion over the spring-neap cycle induce significant variations in the intertidal salinity structure. Observed higher frequency salinity fluctuations demonstrate further the intensity and complexity of the salt-freshwater mixing process. In contrast with the salinity variations, fresh groundwater was found to discharge around a distinct intertidal beach slope break throughout the spring-neap period. This suggests that the slope break may affect significantly groundwater flow and salt transport near the shore. Measurements of pH and dissolved oxygen distributions revealed important biogeochemical zonations in the system. These zonations are expected to strongly influence the fate of many reactive chemicals in the nearshore aquifer and their subsequent discharge to coastal waters.

**Citation:** Robinson, C., B. Gibbes, H. Carey, and L. Li (2007), Salt-freshwater dynamics in a subterranean estuary over a spring-neap tidal cycle, *J. Geophys. Res.*, *112*, C09007, doi:10.1029/2006JC003888.

## 1. Introduction

[2] Submarine groundwater discharge (SGD) provides a significant transport pathway for terrestrial contaminants entering coastal waters [*Simmons*, 1992; *Church*, 1996; *Moore*, 1996]. SGD consists of both terrestrially derived fresh groundwater and seawater recirculating across the aquifer-ocean interface [*Taniguchi et al.*, 2002]. The latter often constitutes a large portion of the total SGD [*Li et al.*, 1999; *Burnett et al.*, 2003; *Prieto and Destouni*, 2005; *Boehm et al.*, 2006]. Recirculating seawater is an important component mainly because it transports not only salt but also other chemicals from the ocean into the aquifer. Near the shore, mixing of recirculating seawater with discharging fresh groundwater creates an active biogeochemical reaction zone. This zone has been shown to significantly influence the fate of chemicals and fluxes from the aquifer to coastal waters [*Moore*, 1999; *Charette and Sholkovitz*, 2002; *Ullman et al.*, 2003; *Charette and Sholkovitz*, 2006]. The salt-freshwater mixing also affects the habitat condition in the interstitial beach environment for a wide range of flora and fauna [*McLachlan and Turner*, 1994; *Miller and Ullman*, 2004; *Zipperle and Reise*, 2005]. As its function may be compared to that of a surface estuary, this mixing and reaction zone has been termed a "subterranean estuary" [*Moore*, 1999]. In contrast to the large amount of literature on the flow, transport and reaction processes in surface estuaries, subterranean estuaries are not well studied.

[3] Oceanic forcing (waves and tides) in the presence of fresh groundwater discharge results in dynamic and complex flows and salt transport in the subterranean estuary [*Robinson et al.*, 1998; *Robinson et al.*, 2006]. Under these forcing conditions, the salinity structure in the nearshore aquifer is characterized by two distinct saline plumes: the classical saltwater wedge and an upper saline plume [*Ataie-Ashtiani et al.*, 1999; *Boufadel*, 2000; *Turner and Acworth*, 2004; *Vandenbohede and Lebbe*, 2005; *Westbrook et al.*, 2005; *Robinson et al.*, 2006] (Figure 1). These two plumes confine a freshwater discharge "tube", whereby fresh groundwater discharges near the low tide mark [*Boufadel*, 2000; *Robinson et al.*, 2006]. The saltwater wedge has been the focus of numerous investigations since the work of *Ghyben* [1899] and *Herzberg* [1901]. It develops due to density variations between seawater and fresh groundwater. Hydrodynamic dispersion of salt across the salt-freshwater transition zone sets up convective seawater circulation through the wedge (Figure 1) [*Cooper*, 1959]. In contrast, the upper saline plume is formed primarily by tides and waves. These oceanic oscillations drive seawater recirculation across the aquifer-ocean interface at significant rates

[1] Environmental Engineering Division, School of Engineering, The University of Queensland, St. Lucia, Australia.
[2] Centre for Eco-Environmental Modelling, Hohai University, Nanjing, China.


0148-0227/07/2006JC003888

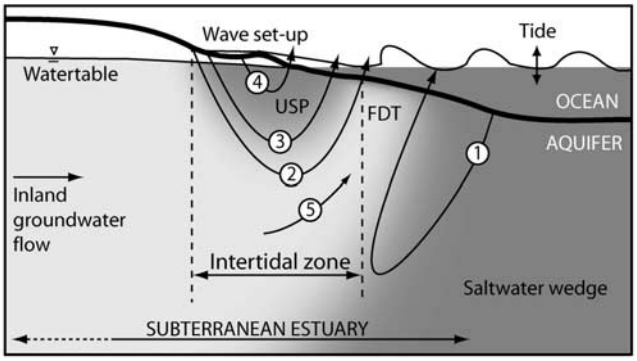


**Figure 1.** Conceptual model of the subterranean estuary system including major nearshore flow processes: (1) density-driven circulation, (2) tide-induced circulation, (3) wave set-up induced circulation, (4) local circulation due to wave-bed form interaction, and (5) fresh groundwater discharge. Shading (grey-scale) depicts typical salinity distribution with an upper saline plume (USP), the classical saltwater wedge and the freshwater discharge "tube" (FDT) in-between. This figure is based on Figure 2 of *Robinson et al.* [2007].

compared with the fresh groundwater discharge [*Li et al.*, 1999]. The tidal action on a sloping beach induces a tide-averaged circulation cell, whereby water infiltrates the beach in the upper intertidal zone and exfiltrates near the low tide mark (Figure 1) [*Mango et al.*, 2004; *Mao et al.*, 2006; *Robinson et al.*, 2006; *Werner and Lockington*, 2006]. Wave set-up also drives seawater circulation through the nearshore aquifer with infiltration at the maximum runup point and exfiltration near the wave breaking point (Figure 1) [*Longuet-Higgins*, 1983; *Li and Barry*, 2000]. Advective salt transport associated with these circulations leads to the development of the upper saline plume [*Robinson et al.*, 2006].

[4] A recent numerical study has shown that as the relative magnitude of the inland (fresh groundwater discharge) to oceanic forcing changes, the salinity stratification and salt-freshwater mixing in the nearshore aquifer vary [*Robinson et al.*, 2007]. For example, as the tidal forcing (i.e., amplitude) increases relative to the fresh groundwater discharge, the tidal circulation cell and thus the upper saline plume expand. This leads to increased salt-freshwater mixing in the system with the freshwater discharge "tube" becoming less profound or nonexistent [*Robinson et al.*, 2007]. Based on these results it is expected that the salinity distribution and mixing conditions in the subterranean estuary would respond to temporal variations in forcing such as variations of the tidal range over the spring-neap cycle and seasonal changes in the inland hydrologic condition.

[5] Previous field observations provide some insight into temporal salinity variations in the nearshore aquifer. Seasonal variations in net fresh groundwater discharge have been shown to drive a shift in the transition zone of the saltwater wedge [*Michael et al.*, 2005] and alter the intertidal salinity structure (i.e., configuration of the upper saline plume) [*Staver and Brinsfield*, 1996; *Robinson et al.*, 1998]. Seepage meter measurements have revealed seasonal, spring-neap and semi-diurnal fluctuations in the salinity of discharging groundwater, thus providing an indication of salinity and flow variations at these time-scales [*Michael et al.*, 2005; *Taniguchi et al.*, 2006]. Salinity measurements by *Cartwright et al.* [2004], landward of the intertidal region, demonstrated significant oscillations (of the order of several meters) in the interface of the saltwater wedge induced by an offshore storm. However, they observed no interface movement in response to semi-diurnal or spring-neap tidal fluctuations.

[6] Despite these studies, there is no existing field data examining the response of the intertidal groundwater salinity structure to oceanic forcing. Previous field studies provide only a "snapshot" of the salinity structure in the subterranean estuary over a relatively short deployment period [*Staver and Brinsfield*, 1996; *Robinson et al.*, 1998; *Ullman et al.*, 2003; *Turner and Acworth*, 2004; *Westbrook et al.*, 2005; *Charette and Sholkovitz*, 2006]. Nevertheless, understanding the salt-freshwater dynamics over different time-scales is crucial for predicting the intensity of mixing in the intertidal subterranean estuary and hence the fate of subsurface contaminants discharging to coastal waters.

[7] In addition to the significance of salt transport in the subterranean estuary, recent geochemical studies have revealed that redox and pH transitions at the mixing zone create important biogeochemical zonations [*Charette and Sholkovitz*, 2002; *Slomp and Cappellen*, 2004; *Spiteri et al.*, 2005]. By controlling reactions within the subterranean estuary, these zonations have been shown to have a significant influence on the distribution of metals and nutrients in the system. For instance, field measurements in Waquoit Bay (Cape Cod) have revealed that Fe and Mn (hydr)oxides form as terrestrial (reduced) groundwater mixes with oxygenated seawater in the subterranean estuary prior to discharge [*Charette and Sholkovitz*, 2002]. The accumulation of these (hydr)oxides was shown to form an "iron curtain" which acts as a geochemical barrier retaining dissolved chemical species including P, Th and Ba. Despite the potential significance of the pH and dissolved oxygen (DO) transitions, measurements of these physiochemical parameters in the subterranean estuary are rare [*Charette and Sholkovitz*, 2006]. To the authors' knowledge, temporal variations of pH and DO in the subterranean estuary in response to oceanic forcing have not yet been examined.

[8] Here, we present field measurements of spatial and temporal variations of salinity, DO and pH in a tidally influenced subterranean estuary. Monitoring was conducted over a 15-day period in order to capture the spring-neap tidal cycle. Measurements of vertical specific discharge are also shown to provide insight into the physical flow processes driving salt transport in the system. To further assist the analysis, a density-dependent groundwater flow model is developed to simulate the field conditions, in particular, the spring-neap tidal oscillations and fresh groundwater discharge. Based on the data we identify the influence of different forcing mechanisms on the salt-

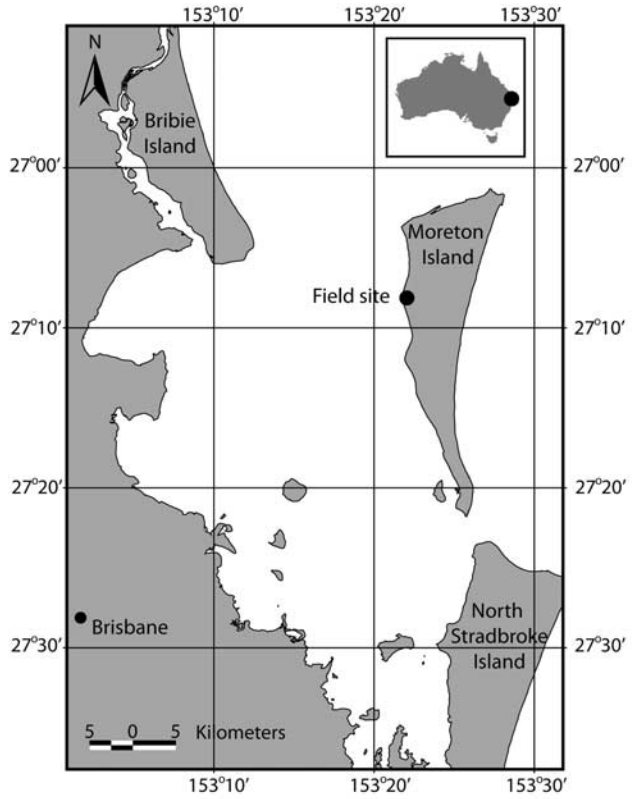


**Figure 2.** Location of field site.

freshwater dynamics and the time-scales of mixing in the intertidal subterranean estuary.

## 2. Field Description and Methodology

### 2.1. Field Site

[9] Field data was collected at a sandy meso-tidal beach on the west coast of Moreton Island, Australia (27°08′39.0″S, 153°21′54.0″E; Figure 2). Groundwater and seawater interaction is of particular interest in this region because large blooms of the toxic marine cyanobacterium *Lyngbya majuscula* have been observed within the surrounding Moreton Bay in recent years [*O'Neil and Dennison*, 2005]. Elevated iron concentrations associated with the groundwater discharge into the bay have been implicated as a causal factor in development of these nuisance blooms [*O'Neil and Dennison*, 2005; *Watkinson et al.*, 2005]. Moreton Island is a relatively pristine environment subject to minimal anthropogenic impact. As a result, it is an ideal control site for studying groundwater discharge into the bay and the major mechanisms driving chemical transport and transformation in a subterranean estuary.

[10] Sampling was conducted over a 17-day period from 7–23 July 2005. This monitoring period captured one complete spring-neap cycle. The tide typically provides the dominant oceanic forcing at the site with waves providing additional forcing during storms and under winter westerly wind conditions. Figure 3 shows the oceanic forcing leading up to and during the field deployment. The tidal range varied from approximately 1.1 m at the neap tide (8 elapsed days) to 2.2 m at the spring tide (14 elapsed days). The wave forcing was small throughout the monitoring period with the exception of an increase in the wave height ($H_{sig}$) to around 1.1 m at 3.5 elapsed days (Figure 3b). This increase in wave height corresponded with a strong westerly wind and lasted for less than 12 h. Rainfall data from the Cape Moreton weather station, 12 km north of the site, indicated that although there was significant rainfall in the months leading up to the deployment (260 mm from 1 May–6 July), the rainfall was minimal during the monitoring period (12 mm from 7–23 July, Figure 4).

[11] Sand levels were surveyed each day during the deployment. The overall beach morphology was characterized by a relatively steep (slope ~0.05) upper intertidal region and flat (~0.01) spring lower intertidal and subtidal region (Figure 5). These two regions were separated by a distinct break in slope, located around the neap low tide mark ($x \approx 51.5$ m BM). A berm and trough formed in the intertidal region on 4 elapsed days in response to the increase in wave climate. The berm slowly migrated landward over the following four days. Recent field measurements have shown that the interaction of oceanic oscillations with complex beach morphology can affect groundwater flow patterns and salt transport in the intertidal region (Figure 1) [*Robinson et al.*, 2006]. While the intertidal slope break is expected to influence considerably the beach's drainage characteristics and thus groundwater flow behavior [*Turner*, 1993a, 1993b; *Li et al.*, 2002], the effects of the berm development on the flow and transport processes are likely more localized.

[12] Sediment samples were collected from various locations and depths through the subtidal, intertidal and inland

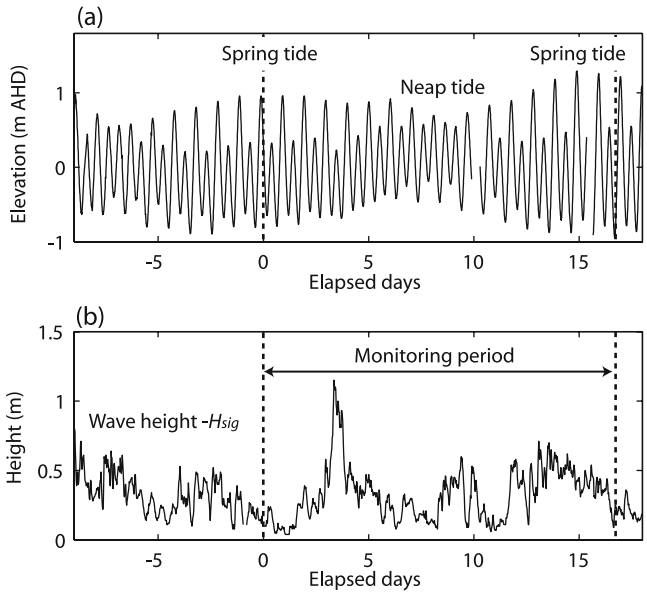


**Figure 3.** (a) Tide data from Brisbane Bar tidal station located 40 km southwest of the field site and (b) wave data from Moreton Bay waverider buoy located 25 km southwest of the field site. Tide data was provided by Maritime Safety Queensland and wave data from the State of Queensland's Environmental Protection Agency. Elapsed days are defined as number of days since 7 July 2005 00:00.

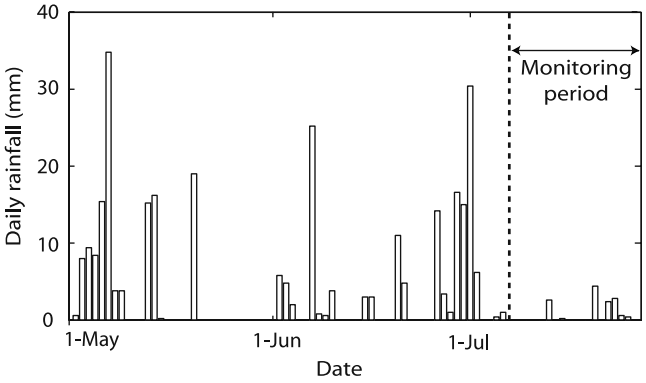


**Figure 4.** Daily rainfall totals for 2 months prior to and during the monitoring period at Cape Moreton weather station, 12 km north of the field site. Data was provided by the Bureau of Meteorology, Australia.

regions. Sediment size analyses showed that the aquifer is relatively homogeneous composed of well-sorted quartz sand with $d_{50}$ ranging from 0.34 to 0.45 mm and $d_{90}/d_{10}$ from 1.94 to 2.56. Sediment sorting generally improved in the seaward direction. Bail and slug tests were also conducted in the intertidal and inland regions. The head recovery curves, analyzed using the *Hvorslev method* [1951], gave estimates of the sediment hydraulic conductivity in the range of $23-34$ m d$^{-1}$.

### 2.2. Field Methods

[13] A single shore-normal monitoring transect was installed since the alongshore variability at the site was negligible. The transect extended from 120 m landward of the spring high tide mark to 10 m seaward of the spring low tide mark (Figure 5). The locations of the monitoring equipment were surveyed in reference to a local permanent benchmark (BM) horizontally and the Australian Height Datum (AHD) vertically.

[14] Piezometers were installed along the transect to monitor the elevation of the water table and mean seawater surface. Landward of the intertidal region, piezometers were of a simple standpipe design, constructed from PVC pipe ($\phi$50 mm) and screened at the base. As vertical flows are negligible landward of the high tide mark, piezometers could be used there to measure the water table elevation instead of fully slotted wells. Manual water level measurements were made using a conduction dipmeter. In the intertidal and subtidal regions, piezometers were constructed from clear poly carbonate tubing ($\phi$32 mm) with an external measuring tape for water level reading. The bottom opening of these piezometers was packed with filter cloth so as to dampen high-frequency oscillations from individual wave and swash events, and hence provide data on the mean seawater surface [*Cartwright and Nielsen*, 2001]. Water levels in piezometers were recorded manually every 30 min for eleven 13-h monitoring periods. The beach face position of the water table's exit point (intersection of the water table with the beach face) and the wave runup limit were also recorded every 30 min. We determined the exit point of the water table as the boundary between the landward matted (dry) sand surface and seaward shiny, saturated sand surface [*Cartwright and Nielsen*, 2001]. The wave runup limit was determined as the maximum (most landward) position on the beach face that the wave runup reached during the first 5 min of each 30 minute measurement period.

[15] Pore water samples were collected through the intertidal region using six multilevel sampling spears (Figure 5). These spears, adapted from the designs of *Pickens et al.* [1978] and *Martin et al.* [2003], were constructed from $\phi$25 mm stainless steel pipe. Each spear had 21 sampling ports spaced at 0.1 m intervals. To increase the spatial coverage of the sampling, single-port sampling spears were also installed in the intertidal and subtidal regions (Figure 5). Pore water samples were collected using 60 mL syringes. The volume of sample was minimized to reduce the disturbance on the surrounding pore water. The radius of the capture zone (based on the volume of "dead water" in the sample line and sample volume) was calculated and checked to ensure that the collected samples accurately represented the pore water at the sampling port and that there was no cross-contamination between ports. Extracted samples were directly transferred to a flow cell and analyzed for salinity, pH, DO and temperature using a water quality meter (YSI 556 MPS). Care was taken to ensure that the sample was not aerated prior to analysis. The water quality meter was calibrated before and after each sampling event. Samples were extracted from every multilevel and single-port sampling spear at least once each day for the duration of the field deployment. A complete profile from all spears required at least 6 h of sampling. As a result the spatial pore water data presented does not represent synchronous measurements, but rather the data has been collated over an entire day.

[16] Six self-logging transducers (In situ LTS TROLL 9000) recording pressure, salinity and temperature were also installed in three vertical arrays in the intertidal region (Figure 5). These transducers provided high frequency (0.167 Hz) and continuous measurements of local pore water pressure and salinity over the deployment period. Each transducer was installed in an individual screened chamber at the bottom of a $\phi$50 mm PVC pipe. This installation method allowed for easy equipment installation and removal, whilst maximizing the sensors' contact with pore water and thus the accuracy of readings. The instruments were installed alongside the sampling spears for intercalibration and verification of the manual extractive and electronic in situ salinity measurement techniques. Installation of transducers in vertical arrays allowed for calculation of non-dimensional vertical specific discharge (vertical specific flows/sediment hydraulic conductivity) from which the magnitude of vertical flows could be inferred.

[17] The non-dimensional vertical specific discharge between the shallow and deep transducers was calculated by:

$$\text{Non} - \text{dimensional vertical specific discharge}(t) = \frac{\left[\frac{P_1(t)}{\rho_f g} - \frac{P_2(t)}{\rho_f g}\right]}{z_1 - z_2} + \frac{\rho_1(t) + \rho_2(t)}{2\rho_f}, \quad (1)$$

where $P$(Pa) is the pore water pressure at time $t$, subscripts 1 and 2 denote the shallow and deep transducers respectively,

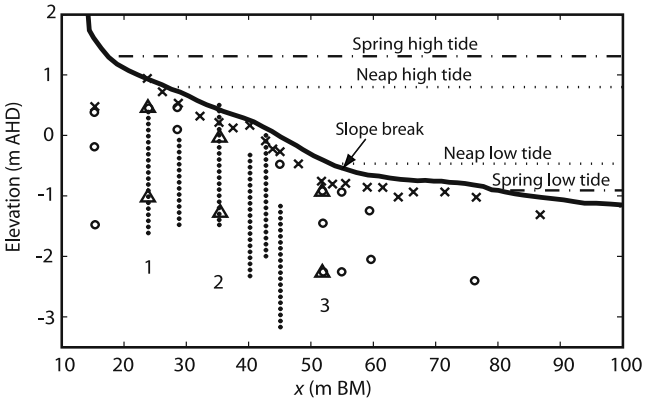


**Figure 5.** Cross-sectional view of field site showing location of instrumentation: stilling piezometers (×), multilevel sampling spear ports (●), single sampling spear ports (○) and LTS TROLL 9000 (△). Beach morphology on 11 elapsed days (—), spring high and low tide levels (14 elapsed days, - · -), and neap high and low tide levels (8 elapsed days, · · · ·) are also shown. The LTS TROLL 9000 vertical arrays are numbered (1, 2 and 3). Seven piezometers were installed further inland between $x = 0$ and $x = -95.1$ m BM. BM refers to a local permanent benchmark, where the origin of the $x$ axis is located.

$z$ (m) is the elevation of the pressure sensor, $\rho_f$ (kg m$^{-3}$) is the freshwater density and $\rho$ (kg m$^{-3}$) is the local pore water density at time $t$ which was calculated based on the salinity readings. Note that equation (1) in a finite difference form is identical to the specific discharge equation based on the equivalent freshwater head and a density correction term; for example, equation (32) of *Guo and Langevin* [2002]. The calculated raw non-dimensional vertical specific discharges were smoothed using a 10-minute running average. This averaging period allowed for the removal of high frequency noise from individual wave and swash events while preserving the details of the dynamic behavior associated with tidal forcing.

### 2.3. Numerical Model

[18] A variable-density groundwater model of the field conditions was developed to simulate flows and salt transport in the intertidal subterranean estuary in response to tides. The purpose of the modeling was to enhance understanding of observed salinity fluctuations and provide insight into water exchange and groundwater flows driving these fluctuations over the spring-neap tidal cycle. The model is unique in examining the influence of complex tidal forcing (i.e., multiple tidal constituents) on nearshore groundwater hydrodynamics and salt transport. Previous numerical studies have only investigated the effects of single-constituent tidal forcing [*Ataie-Ashtiani et al.*, 1999; *Robinson and Gallagher*, 1999; *Mao et al.*, 2006; *Werner and Lockington*, 2006; *Robinson et al.*, 2007].

[19] Simulations were performed using the density-dependent groundwater flow code, SEAWAT 2000 [*Langevin et al.*, 2003]. The numerical model used was a modified version of that presented by *Robinson et al.* [2007]. The model is described briefly in the following and the reader is referred to *Robinson et al.* [2007] for further details of the model and its development. Tidal forcing across the sloping beach boundary was simulated using a two zone model with a surface water zone and an aquifer zone. A schematic of the model domain including boundary conditions and parameters used is shown in Figure 6. The beach profile was based on the sand level survey data from 11 elapsed days and was kept constant through the simulation. This simplification was appropriate as the beach morphology remained relatively stable during the field deployment with the exception of the berm which formed in the intertidal region on 4 elapsed days. As the influence of the berm development on the flow and trans-

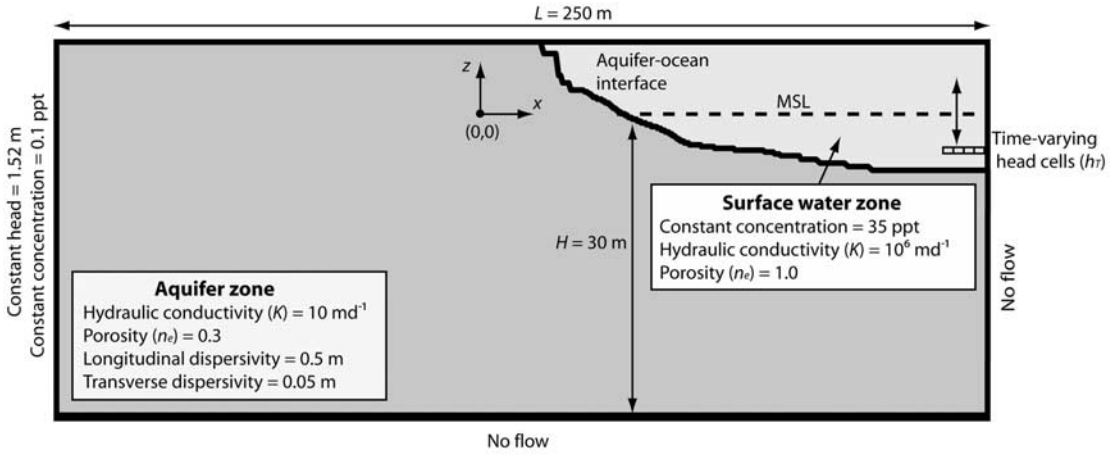


**Figure 6.** Model geometry, boundary conditions and basic parameter set. The model domain is divided into a surface water zone and an aquifer zone. Constant head ($h$ = 1.52 m AHD) and concentration ($C$ = 0.1 ppt) implemented at inland boundary are the averaged values over the monitoring period. Beach morphology (—) corresponds with sand level survey data from 11 elapsed days. The coordinate origin (0, 0) is based on a local permanent benchmark (BM) horizontally and the Australian Height Datum (AHD) vertically. The intersection of the mean sea level (MSL) with the beach face occurs at $x$ = 44.5 m, $z$ = 0 m.

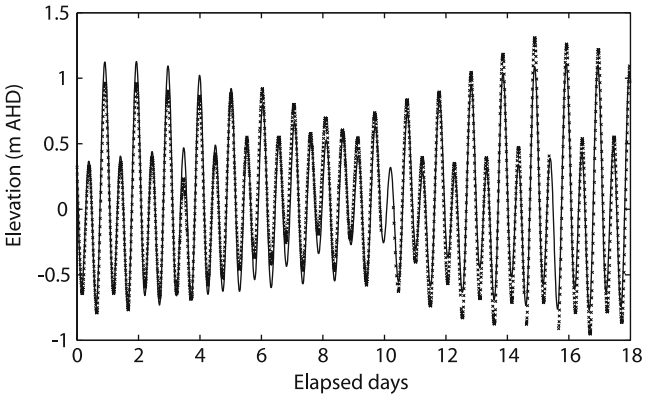


**Figure 7.** Measured tide data from Brisbane Bar tidal station (×) and synthetic tidal signal (—) used to simulate tidal forcing in the numerical model.

port behavior was localized, these morphological changes were not included in the numerical simulation. A constant hydraulic conductivity of 10 m $d^{-1}$ was used throughout the aquifer zone. This value was determined by calibrating the model such that the predicted spatial salinity distribution corresponded reasonably with the overall salinity distribution measured in the field. This value is similar to the field measurements (23–34 m $d^{-1}$, section 2.1).

[20] To simulate the field conditions, a Dirichlet condition was applied at the inland boundary. The position of this boundary corresponded with the location of the furthest inland piezometer at $x = -95.1$ m BM. The water table elevation at this location fluctuated by less than 5 cm through the monitoring period. As such, a constant head (average value = 1.52 m AHD) was applied at this boundary.

[21] A multiple constituent tidal signal was implemented via time-varying head cells in the surface water zone (Figure 6). A synthetic signal was developed to match the tides through the deployment period. To generate the signal, the following tidal constituents were considered: principle solar semi-diurnal ($S_2$), principle lunar semi-diurnal ($M_2$), solar diurnal ($S_1$) and lunar diurnal ($O_1$). The fitting equation used was:

$$h_T = \mathrm{MSL} + \sum_{i=1}^{4} A_i \cos(\omega_i t - \delta_i), \qquad (2)$$

where $h_T$ (m AHD) is the synthetic tidal signal, MSL (m AHD) is the mean sea level, $A_i$ (m) and $\delta_i$ (rad) are the amplitude and phase of tidal constituent $i$, and $\omega_i$ (rad $s^{-1}$) is the corresponding tidal frequency which is known a priori [*Pugh*, 1987]. A comparison of the measured tide data with the synthetic tidal signal is shown in Figure 7. The measured tide data could not be directly simulated as a continuous signal was required to run the model for multiple spring-neap cycles. Simulation of tidal oscillations was computationally intensive so the model was initially run to steady state with no tide. The tidal signal was then introduced and the model was run until the quasi-steady state (i.e., the periodic solution) was reached with respect to concentrations and flow. This solution was obtained after approximately 30 spring-neap cycles. It is assumed that the quasi-steady state result is representative of the field condition. Grid independence tests were performed to ensure a converged numerical solution.

## 3. Results and Discussion

### 3.1. Measured Spatial and Temporal Variations of Salinity

[22] Salinity measurements revealed a well-defined intertidal subterranean estuary with significant mixing between recirculating seawater and discharging fresh groundwater (Figure 8). An upper saline plume composed of mixed waters was evident in the upper and mid intertidal regions. Although the salt distribution was complex, the salinity generally decreased with depth in this upper plume. Fresh groundwater confined between the upper saline plume and the saltwater wedge discharged around the distinct beach slope break located near the neap low tide mark.

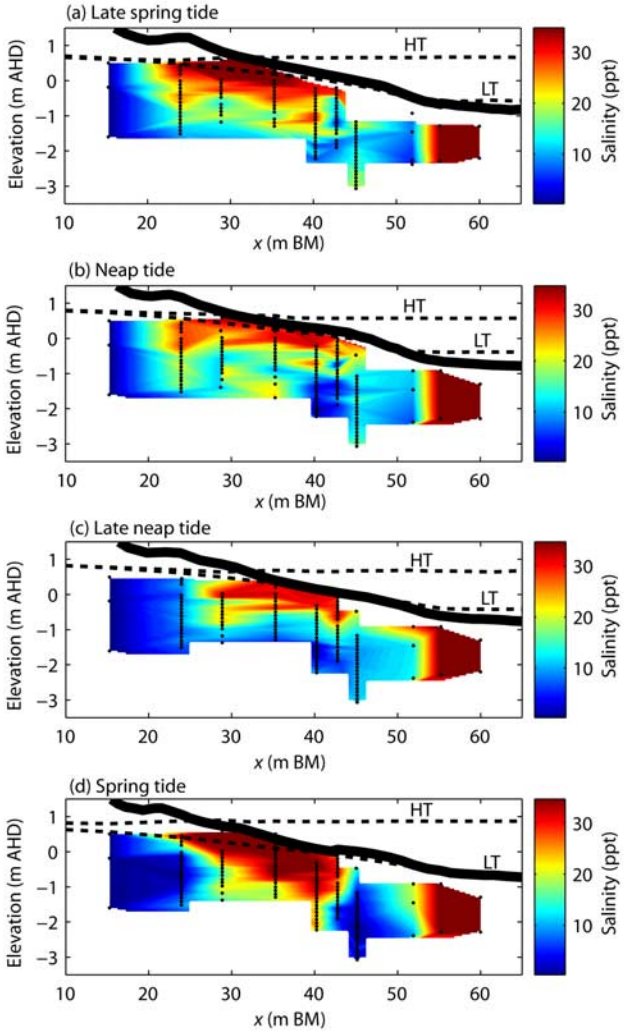


**Figure 8.** Spatial salinity distributions measured on (a) 4 elapsed days (b) 8 elapsed days (c) 11 elapsed days and (d) 14 elapsed days. Sand levels (—) and maximum high tide (HT) and low tide (LT) water levels recorded (– –) for each day are also shown.

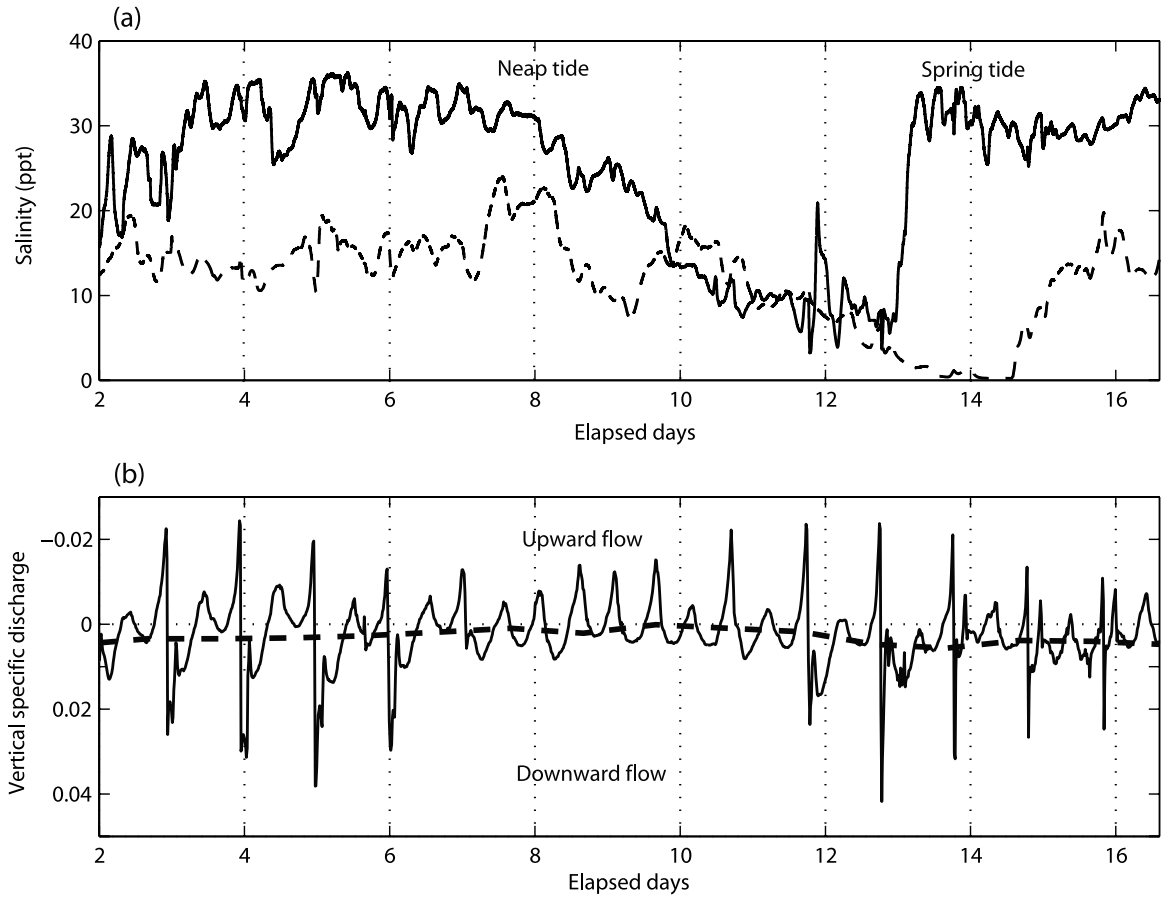


**Figure 9.** (a) Salinity data recorded by transducers LTS 1S (—, $x$ = 23.9 m BM, $z$ = 0.45 m AHD, ~0.48 m below sand surface) and LTS 1D (· · ·, $x$ = 23.9 m BM, $z$ = −1.03 m AHD, ~1.96 m below sand surface). (b) Non-dimensional vertical specific discharge between LTS 1S and LTS 1D from 2 to 16.6 elapsed days (—). Residual (averaged over 24 h) non-dimensional vertical specific discharge (– –) is also shown. Note that the vertical axis in (b) is reverse and a negative non-dimensional specific discharge indicates upward flow. Elapsed days are defined as number of days since 7 July 2005 00:00.

[23] The salinities in the upper saline plume changed significantly over the 17-day sampling period. The plume was well-developed around the spring tides at the beginning and end of the monitoring period (Figures 8a and 8d) with high salinities (>30 ppt) measured to depths of approximately 1 and 1.3 m below the sand surface respectively. The plume penetration depth decreased at the neap tide with high salinities measured to only 0.5 m below the sand surface (Figure 8b). The horizontal extent of the upper saline plume also decreased on the neap tide and following days (Figures 8b and 8c).

[24] Continuous salinity and non-dimensional vertical specific discharge data collected by the LTS transducer arrays provided further insight into these temporal salinity variations in the intertidal region. The variation in horizontal extent of the upper plume over the spring-neap period was captured by LTS Array 1 ($x$ = 23.9 m BM, Figure 9a). This array was located in the upper intertidal region during the spring tide (2–7 and 11.5–16.5 elapsed days), but landward of the maximum runup limit during the neap tide (7–11.5 elapsed days). The shallow transducer (LTS 1S) recorded a consistently higher salinity than the deep transducer (LTS 1D), corresponding to the inverted salinity gradient in the upper saline plume (Figure 8). Around the initial spring tide, the salinity was high at LTS 1S, fluctuating around 32 ppt. Strong downward flows recorded as the runup limit and shoreline passed the transducer's location on the rising tide (2.95, 4.0 and 4.97 and 6.0 elapsed days; Figure 9b) indicate that this high salinity was likely due to the infiltration of seawater at the transducer's location and further landward. As the neap tide approached, the shoreline excursion (i.e., distance between the high tide mark and low tide mark) was reduced; and seawater no longer infiltrated into the beach at or landward of LTS 1S. This resulted in a gradual decrease in the salinity at LTS 1S. However, as the spring tide approached, the runup limit and shoreline again passed the transducer's location, and the salinity increased sharply (11.84 and 12.77 elapsed days, Figure 9). To examine the net flow effect, the instantaneous non-dimensional vertical specific discharge was averaged over a 24-h period. The residual (averaged) non-dimensional vertical specific discharge revealed a net downward flow at the transducers' location around the spring tide (maximum residual non-dimensional specific discharge ~0.005 at 13.5 elapsed days). This was likely caused by infiltration associated with the tidal and wave set-up circulations. In

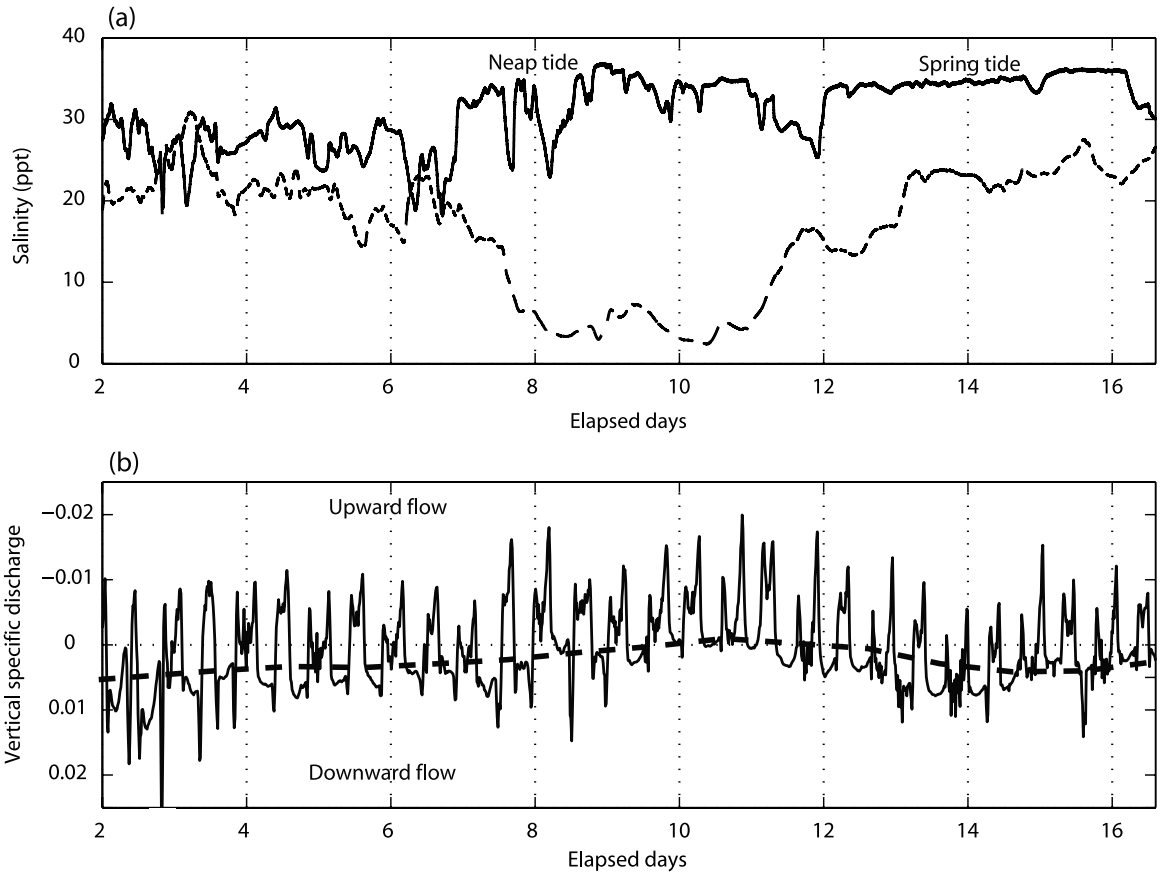


**Figure 10.** (a) Salinity data recorded by transducers LTS 2S (—, $x$ = 35.1 m BM, $z$ = 0.02 m AHD, ∼0.52 m below sand surface) and LTS 2D (· · ·, $x$ = 35.1 m BM, $z$ = −1.29 m AHD, ∼1.83 m below sand surface). (b) Non-dimensional vertical specific discharge between LTS 2S and LTS 2D from 2 to 16.6 elapsed days (—). Residual (averaged over 24 h) non-dimensional vertical specific discharge (– –) is also shown. Note that the vertical axis in (b) is reverse and a negative non-dimensional specific discharge indicates upward flow. Elapsed days are defined as number of days since 7 July 2005 00:00.

contrast, the residual vertical specific discharge was negligible during the neap tide when the transducers were landward of the intertidal region. The salinity at LTS 1D also varied in response to the spring-neap forcing (Figure 9a). The salinity at LTS 1D was lowest (∼1.5 ppt) around 14 elapsed days compared with 12 elapsed days for LTS 1S. This suggests a delayed response with depth with a phase lag of ∼2 d between the spring-neap oscillations at LTS 1S and LTS 1D.

[25] The vertical contraction and expansion of the upper saline plume over the spring-neap period revealed by the manual measurements (Figure 8), was also demonstrated by the salinity time series from the deep transducer in LTS Array 2 (LTS 2D, Figure 10a). This transducer, located in the mid-upper intertidal region ($x$ = 35.1 m BM), measured a strong spring-neap oscillation reaching ∼25 ppt during the spring tide and decreasing to ∼3 ppt at the neap tide. In comparison, the salinity recorded by LTS 2S, located in the shallow area of the upper saline plume, showed no significant spring-neap variations but was dominated by higher frequency fluctuations. The salinity was high ranging between 20 and 35 ppt. The non-dimensional vertical specific discharge data showed significant downward and upward flows through the tidal cycles at this location (Figure 10b). While the residual specific discharge revealed negligible net vertical flow from 9–12.5 elapsed days, the net vertical flow was downward over the remainder of the spring-neap period. This net downward flow is consistent with the tidal circulation cell which operates through intertidal regions: downward flow dominates in the upper intertidal region, horizontal flow in the mid intertidal region and upward flow in the lower intertidal region [*Mango et al.*, 2004; *Robinson et al.*, 2006]. The net downward flow was most profound around the spring tide (14–15 elapsed days) when the tidal range was at its maximum.

[26] Numerical simulations have previously shown that when an unconfined aquifer is subject to single-constituent tidal forcing across a mildly sloping planar beach, fresh groundwater discharges around the low tide mark, confined between the tide-induced upper saline plume and lower saltwater wedge [*Robinson et al.*, 2007]. Based on this result it was anticipated that the freshwater discharge zone would be located between the neap and spring low tide marks and might oscillate landward and seaward over the spring-neap cycle in response to the varying low tide level.

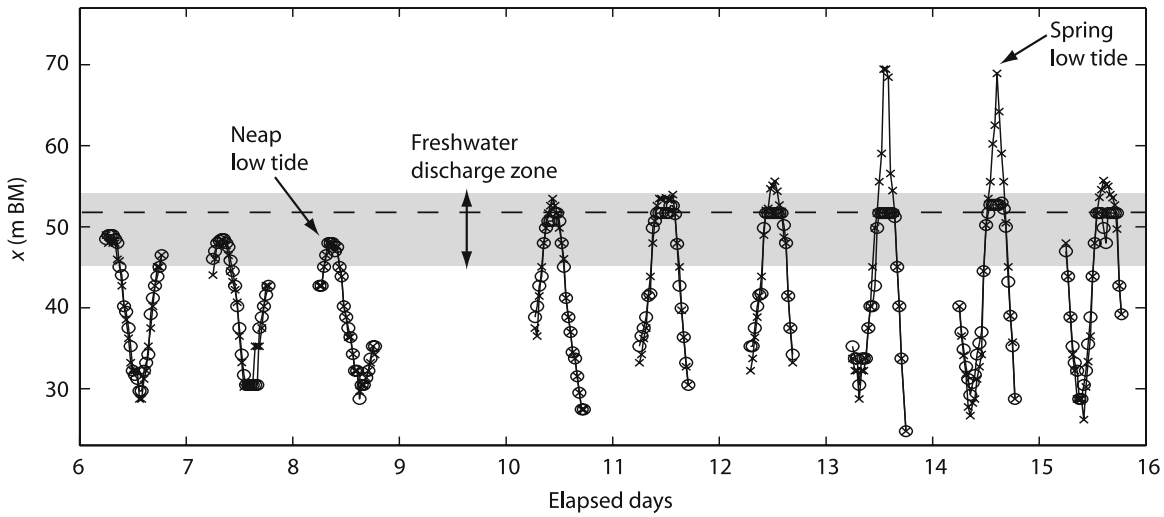


**Figure 11.** Beach face location of the water table's exit point (−○−) and maximum wave runup limit (−×−) every 30 min over nine 13-h manual monitoring periods. The approximate locations of the freshwater discharge zone as revealed by the salinity measurements (grey shading) and slope break (− −) are also shown. Elapsed days are defined as number of days since 7 July 2005 00:00.

Contrary to these expectations and in contrast with the significant salinity variations observed in the mid to upper intertidal region, the location of the freshwater discharge zone remained relatively constant over the monitoring period. The pore water salinity measurements indicated that fresh groundwater discharged between approximately 45–53.5 m, around the distinct beach slope break located near the neap low tide mark, through the spring-neap cycle (Figure 8).

[27] Measurements also showed a relatively constant location of the water table's exit point at low tides over the spring-neap cycle (Figure 11). Around the neap tide, the low tide mark was slightly landward of the slope break and the water table's exit point was coupled with the runup limit over the tidal cycle. As the spring tide approached, the low tide mark shifted seaward away from the slope break by over 15 m. However, the exit point's seaward movement during the ebb tide was constrained by the slope break. A mass balance around the exit point suggests that the exit point's movement was largely controlled by the difference between the water table slope (landward of the exit point) and the beach face slope (seaward of the exit point). The water table slope determined the rate of inflow from the aquifer to the exit point, whereas the beach face slope controlled the rate of outflow from the exit point to the ocean. A smaller water table slope and hence inflow rate led to the fall and seaward movement of the exit point before reaching the slope break. At the slope break, the sudden decrease of the beach slope and hence the outflow rate resulted in greater inflow to the exit point than outflow. As a result, the exit point was retained at the slope break and decoupled with the tide level and the runup limit as the surplus inflow continued until the approach of the rising tide (Figure 11). The influence of intertidal slope breaks on the exit point's movement (i.e., beach drainage characteristics) has previously been discussed by *Turner* [1993a] and *Li et al.* [2002]. Numerical simulations have shown that the seaward movement of the water table's exit point affects the width of the tide-averaged circulation cell and thus upper saline plume [*Robinson et al.*, 2007]. Therefore the measured relatively invariant location of the exit point at low tides (i.e., its seaward limit) may be linked to the observed relatively constant freshwater discharge zone over the spring-neap cycle; both remained around the slope break.

[28] LTS Array 3 was located close to the beach slope break ($x$ = 51.8 m BM). The salinity recorded by LTS 3D was low (<15 ppt, Figure 12a) and a strong residual upward flow was maintained throughout the monitoring period (Figure 12b). This is consistent with the transducer being located in the freshwater discharge "tube". The salinity recorded by LTS3S however was more complicated illustrating the complex and dynamic nature of salt transport in the system. The salinity gradually increased from ~2 to 12 ppt over the first half of the monitoring period prior to a rapid increase in salinity from 7.5 to 29 ppt at 10.4 elapsed days. The spatial salinity measurements (Figure 8) indicated that this transducer was located on the seaward side of the freshwater discharge "tube" over the monitoring period. The rapid increase in salinity, not seen at LTS 3D, could not have been caused by a landward shift in the saltwater wedge. Also, sand levels around the slope break were stable around 6–11 days; therefore, the salinity increase was not driven by morphological changes. Considering that the salinity increase occurred rapidly (over 3 h) and was only evident in the upper transducer (~0.54 m below the sand surface), we hypothesize that the change may have been caused by localized processes such as unstable convective flow. The inverted density gradient between the salty overlying surface water and freshwater discharge zone may have led to the development of instabilities (free convection) in an attempt to restore gravitational stability to the system [*Schincariol and Schwartz*, 1990]. These instabilities manifest as lobe shaped protuberances, also known as fingers, and can cause rapid salt transport and mixing between fresh groundwater and saltwater [*Simmons*

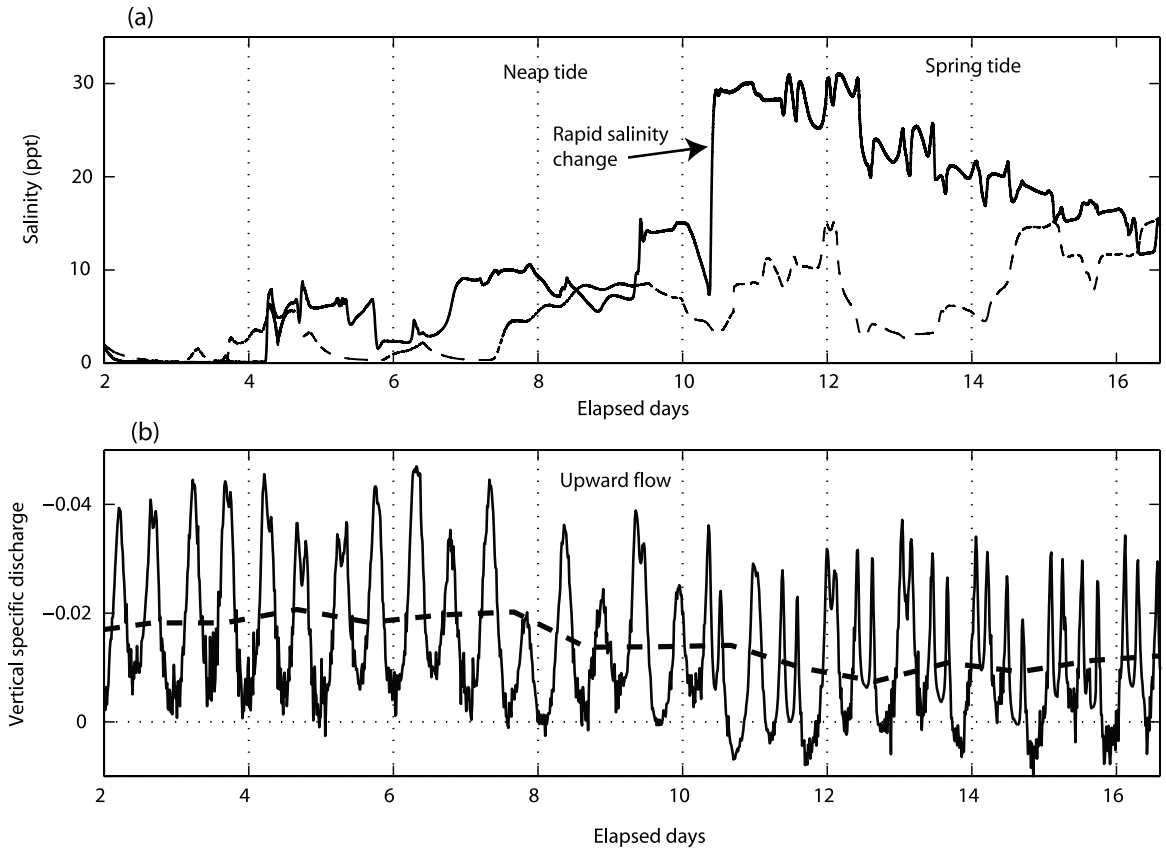


**Figure 12.** (a) Salinity data recorded by transducers LTS 3S (—, $x$ = 51.8 m BM, $z$ = −0.93 m AHD, ∼0.54 m below sand surface) and LTS 3D (· · ·, $x$ = 51.8 m BM, $z$ = −2.27 m AHD, ∼1.87 m below sand surface). (b) Non-dimensional vertical specific discharge between LTS 3S and LTS 3D from 2 to 16.6 elapsed days (—). Residual (averaged over 24 h) non-dimensional vertical specific discharge (– –) is also shown. Note that the vertical axis in (b) is reverse and a negative non-dimensional specific discharge indicates upward flow. Elapsed days are defined as number of days since 7 July 2005 00:00.

*et al.*, 2001]. The Rayleigh number, which describes the ratio of the destabilizing buoyancy force to the stabilizing diffusion/dispersion, is commonly applied in numerical and laboratory experiments to determine the conditions required for the onset of instabilities and their subsequent propagation [*Oostrom et al.*, 1992]. However, the application of the Rayleigh stability criterion to field scale conditions is often hindered by the scale-dependence of the problem and uncertainties associated with the aquifer dispersivities and heterogeneities [*Schincariol*, 1998]. The current data set is not adequate for determining whether the conditions in the freshwater discharge zone would have favored the initiation of instabilities.

[29] High frequency salinity variations are evident in the time series shown in Figures 9a, 10a and 12a in addition to the longer period salinity fluctuations described above. Further investigation of these higher frequency fluctuations through spectral and cross-correlation analyses suggested that these fluctuations were complicated and not simply controlled by the principal forcing mechanisms. The salinity did not vary in direct response to the semi-diurnal tidal signal, nor to changes in the wave climate or beach morphology. Although the absence of strong semi-diurnal fluctuations in salinity, particularly near the freshwater discharge zone, contrasts with recent conceptual models [*Barry and Parlange*, 2004; *Urish*, 2004]; such behavior is supported by numerical simulations conducted by *Ataie-Ashtiani et al.* [1999], *Mao et al.* [2006] and *Robinson et al.* [2007]. The lack of response in the salinity to the intensified wave climate around 3.5 elapsed days is consistent with field observations of *Cartwright et al.* [2004]. They showed that a wave event needs to be of a minimum magnitude and duration to have a noticeable effect on the salinity distribution. The rather complicated high frequency salinity fluctuations reflect the intensity of mixing in the system, which results from complex and dynamic interactions among the tide, waves, beach morphology, aquifer heterogeneities, inland forcing and density variations.

### 3.2. Model Results and Comparison With Field Data

[30] A numerical simulation was conducted to examine the tidal effects on salinity distribution and flow in the intertidal subterranean estuary based on the field conditions. The results corresponded well with the field observations, showing significant variations in the intertidal salinity distribution over the spring-neap period (Figure 13) but little fluctuations within the semi-diurnal cycle. The simulated upper saline plume contracted and expanded over the spring-neap cycle, reaching its largest and smallest extent

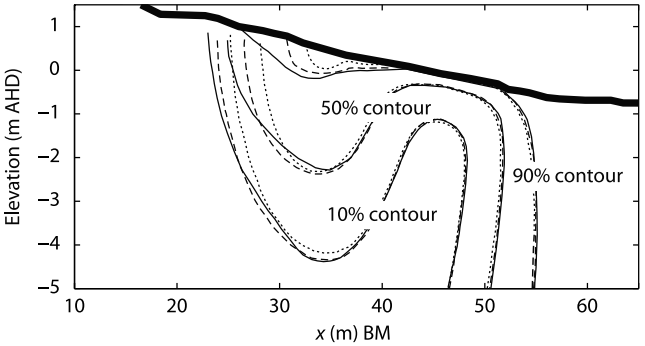


**Figure 13.** Simulated 10%, 50% and 90% seawater salinity contours in the intertidal subterranean estuary on 4 elapsed days (late spring tide, —), 8 elapsed days (neap tide, – –) and 11 elapsed days (late neap tide, · · · ·).

3 days after the spring (4 elapsed days) and neap tides (11 elapsed days) respectively. The phase lag between the spring-neap tidal variations and the salinity fluctuations was also observed in the field (Figures 8, 9a and 10a). Based on the contour of 50% seawater salinity, the landward extent of the simulated upper saline plume decreased by approximately 5 m from 4 to 11 elapsed days. The zone of higher salinity pore water in mid-shallow area of the plume, as represented by the 90% seawater salinity contour, contracted by more than 10 m. The depth of penetration of this higher salinity zone also reduced from 4 to 11 elapsed days (Figure 13). While the simulated horizontal contraction of the plume was consistent with the field data, the reduction in the plume's vertical extent was less than that observed in the field (Figure 8). This under-prediction is particularly evident in the 10% and 50% seawater salinity contours for which the maximum depths did not change considerably over the spring-neap period. The discrepancy was likely due to the complexities of the field system such as the wave effects, and aquifer heterogeneity and anisotropy which were not included in the numerical model. Further research and simulations are required to better understand the influence of these factors on salt-freshwater dynamics in the intertidal subterranean estuary.

[31] The simulated groundwater flows indicated that the reduction in plume size over the neap tide was due to the weakening of the tide-induced circulations through the intertidal region as the tidal forcing decreased (Figure 14). Residual groundwater flows were obtained by extracting the instantaneous, temporally varying flows from the simulation results every 0.1 h and averaging these flows over the period (24 h) between 8–9 elapsed days (neap tide, Figure 14a) and 14–15 elapsed days (spring tide, Figure 14b). The results showed that the circulation cell became narrower and shallower over the neap tide. This is particularly evident in comparing the velocity vectors around $x$ = 25–35 m BM. As a result of the weakened circulation cell, the recirculating seawater and salt were not advected into the upper intertidal region or as deep into the aquifer around the neap tide. Thus the extent of the plume gradually decreased until the spring tide was again approached and the tidal circulations strengthened accordingly.

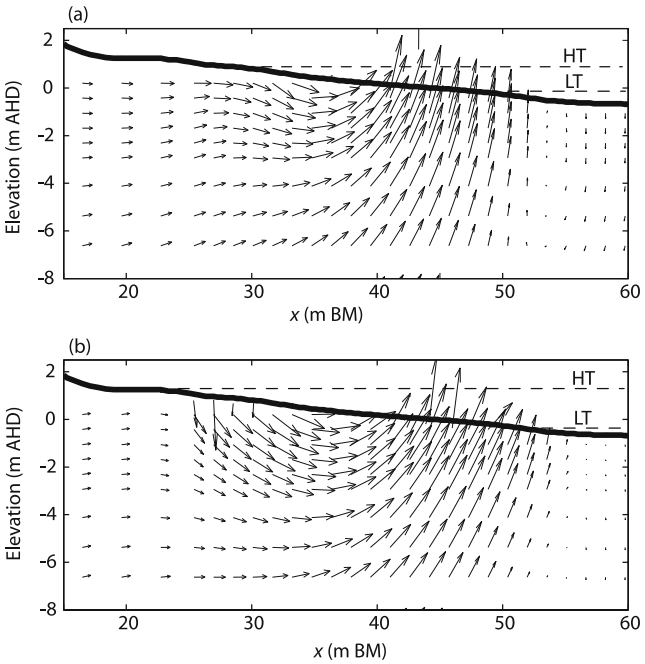


**Figure 14.** Residual (averaged) groundwater flows in the subterranean estuary over the (a) neap tide (between 8–9 elapsed days) and (b) spring tide (between 14–15 elapsed days). HT and LT denote the high tide and low tide levels for each of averaging period.

[32] To further analyze the spring-neap variations of the intertidal aquifer, we examined the spatial water exchange profiles along the aquifer-ocean interface. The total infiltration and exfiltration rates along the interface over 24 h around the spring and neap tides were calculated (Figure 15). The

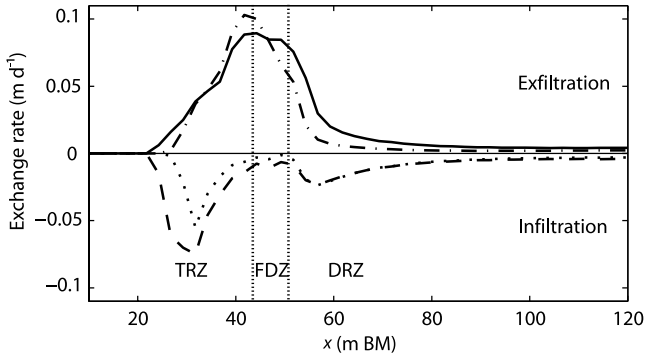


**Figure 15.** Spatial exchange profile along the aquifer-ocean interface over the neap tide and spring tide: total exfiltration (– · –) and infiltration (· · · ·) for period between 8–9 elapsed days (neap tide), total exfiltration (—) and infiltration (– –) for period between 14–15 elapsed days (spring tide). The spatial behavior of infiltration along the interface revealed a tidally driven recirculation zone (TRZ) and density-driven recirculation zone (DRZ) separated by a freshwater discharge zone (FDZ), the location of which remains constant over the spring-neap cycle.

profiles showed three distinct zones similarly for the spring and neap tides: the fresh groundwater discharge zone confined between the tidally driven recirculation zone which operated through the intertidal region and the density-driven recirculation zone which dominated in the subtidal region [*Robinson et al.*, 2007]. The infiltration area in the upper intertidal region was significantly wider during the spring tide than during the neap tide. This was due to the increased shoreline excursion and strength of tidal circulations under the larger forcing conditions. To balance the increased infiltration, the exfiltration area also widened with larger discharge through the lower intertidal and subtidal regions during the spring tide. This increased discharge was also evident in the residual groundwater flows shown in Figure 14. The difference between the spring and neap exchange profiles was consistent with the horizontal contraction of the upper saline plume from the spring to neap tide.

[33] The numerical simulation also predicted a relatively constant freshwater discharge zone between 44–52 m BM around the beach slope break over the spring-neap period, in contrast with the significant salinity variations associated with the upper saline plume (Figure 13). The simulated freshwater discharge "tube" did not shift or contract. These results compared well with the salinity measurements, in particular, the observed discharge zone between 45–53.5 m BM over the monitoring period. A constant freshwater discharge zone characterized by strong exfiltration and negligible infiltration was apparent in the simulated spatial exchange profiles (Figure 15).

[34] The measured residual non-dimensional specific discharge patterns in the upper, mid-upper and lower intertidal zones (Figures 9b, 10b and 12b) compared well with the simulated spatial exchange profiles (Figure 15): net infiltration (downward flow) during the spring tide at LTS Array 1 ($x$ = 23.9 m BM) and LTS Array 2 ($x$ = 35.1 m BM); negligible exchange at LTS Array 1 and negligible net exchange at LTS Array 2 during the neap tide; and strong net discharge (upward flow) at LTS Array 3 ($x$ = 51.8 m BM) throughout the spring-neap period. The complex temporal behaviors of the vertical specific discharge in response to the semi-diurnal tidal forcing, measured in the three different zones, were also consistent with the simulation results. Details of these flow dynamics, including comparison between field and numerical results, have previously been presented by *Robinson et al.* [2006].

[35] To examine the temporal variations in total exchange across the aquifer-ocean interface over the spring-neap period, the infiltration, exfiltration and net discharge rates were integrated over the entire length of the interface. The resulting total exchange rates were found to fluctuate significantly over the spring-neap cycle (Figure 16). The total exfiltration rate decreased from 5.1 to 4.1 $m^3\ d^{-1}\ m^{-1}$ from the spring to neap tide, whereas the total infiltration rate decreased from 3.3 to 2.2 $m^3\ d^{-1}\ m^{-1}$. These results support the field measurements by *Taniguchi* [2002] and *Kim and Hwang* [2002], which revealed significant fluctuations in SGD over the spring-neap period. The net discharge, given by the difference between the total exfiltration and infiltration rates and representing the fresh groundwater flow, remained relatively constant over the period ($\sim$1.9 $m^3\ d^{-1}\ m^{-1}$). The fresh groundwater discharge constituted 37–46% of the total SGD over the spring-neap period. While this freshwater ratio is large compared with other field studies [*Hussain et al.*, 1999; *Kim et al.*, 2003; *Taniguchi and Iwakawa*, 2004], it is difficult to compare results as our calculation only included nearshore seawater recirculation driven by tides and density variations.

### 3.3. Measured Spatial and Temporal Variations of pH and DO

[36] The previous sections have focused on spatial and temporal salinity variations, which provide indications of the extent and time-scales of mixing between fresh and saline waters in the intertidal subterranean estuary. Here we present measurements of pH and DO, two basic physiochemical parameters which have been shown to significantly influence geochemical conditions and the fate of many reactive chemicals in the subterranean estuary [*Charette and Sholkovitz*, 2002; *Slomp and Cappellen*, 2004; *Spiteri et al.*, 2005; *Charette and Sholkovitz*, 2006].

[37] Pore water samples indicated that the inland groundwater at the site was anoxic (DO $\approx$ 0 $mgL^{-1}$) and slightly acidic (pH $\approx$ 5.5), whereas the bay surface water was aerobic (DO $\approx$ 5.6–6.9 $mgL^{-1}$) with a pH around 8. The measured pH and DO distributions revealed significant biogeochemical zonations in the subterranean estuary which were strongly influenced by the exchange and flow processes (Figure 17). The measurements showed zones of high pH (>7.5) associated with the upper saline plume and saltwater wedge (Figures 17a and 17b). In contrast, the pH of the pore water was low in the freshwater discharge "tube" and at the landward and bottom boundaries of the upper saline plume. The pH distribution was relatively stable over the spring-neap cycle. This suggested that although the upper intertidal area freshened during the neap tide with the contraction of the upper saline plume (Figure 8), the biogeochemical processes controlling the pore water pH were insensitive to the salinity variations. The processes that control pore water pH are likely to be complex and depend on interactions with solid phase species [*Appelo and Postma*, 2005; *Spiteri et al.*, 2005]. The system is likely to have established quasi-equilibrium conditions with the solid phase and would require a distinct change in the system to cause variations in pH.

[38] DO measurements showed a single zone of high oxygen content in the upper intertidal region (Figures 17c and 17d). The recirculating seawater maintained a high DO content similar to the surface water near the infiltration zone (i.e., in the upper intertidal region) but oxygen was rapidly depleted along its flow path. We hypothesize that the oxygen was consumed by biogeochemical processes, in particular the oxidation of organic matter and reduced inorganic minerals such as pyrite and siderite [*Hem*, 1985], as seawater circulated through the aquifer. The extent of the high DO zone reduced significantly around the neap tide (Figure 17d). This corresponded with the contraction of the upper saline plume around this time due to the reduced extent of the tidal circulations. Oxygen depletion was the most profound in the subtidal region (saltwater wedge) where very low DO content was measured despite the high salinity (seawater) in this region. This reflects the distinctively different geochemical condition in the saltwater wedge compared with that of the upper saline plume. The low DO content in the saltwater wedge is attributed to the

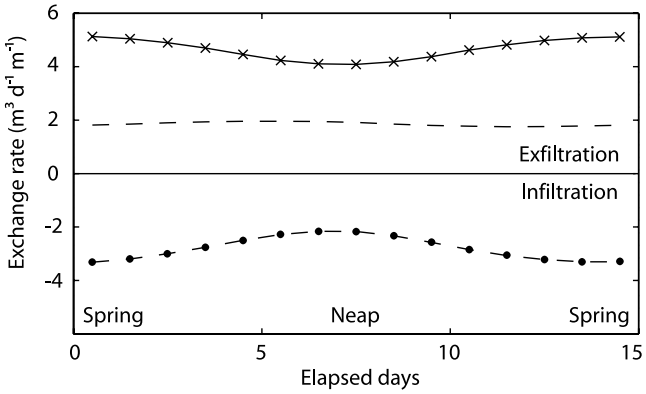


**Figure 16.** Temporal variations in total exfiltration (– × –), infiltration (– ● –) and net discharge (– –) across the simulated aquifer-ocean interface through a spring-neap tidal cycle. Exchange rates shown have been calculated over 24-h periods. A positive exchange rate indicates exfiltration and a negative exchange rate indicates infiltration.

long residence times of seawater associated with density-driven convective flow in this zone [*Robinson et al.*, 2007].

## 4. Conclusions

[39] The subterranean estuary monitored in this study was characterized by an upper saline plume which expanded and contracted in response to changes in tidal forcing over the spring-neap cycle. The plume was composed of mixed waters with a complex and temporally varying salinity structure indicating significant mixing between fresh groundwater and recirculating seawater in this zone. Confined between the upper saline plume and the saltwater wedge, fresh groundwater discharged around a distinct beach slope break located near the neap low tide mark. The location of the freshwater discharge zone was relatively stable over the spring-neap cycle, suggesting a controlling influence of the slope break on the discharge process. Measurements revealed high frequency salinity fluctuations in addition to the dominant lower frequency spring-neap variations. Although the rapid fluctuations were complex and did not directly correlate with the higher frequency forcing mechanisms (i.e., semi-diurnal signal, changes in wave climate or beach morphology), they demonstrated the intensity of mixing in the system and were likely due to the complex, dynamic interactions between oceanic and inland forcing, density variations, beach morphology and aquifer heterogeneities.

[40] The numerical simulation of the field conditions demonstrated that the variations in the intertidal salinity distribution were primarily due to changes in the shoreline excursion and strength of tidal circulations over the spring-neap cycle. The influence of the spring-neap fluctuations on the subterranean estuary was exemplified in the trend of decreasing water exchange across the aquifer-ocean interface from the spring to neap tide.

[41] In addition to salinity measurements, pH and DO profiles revealed significant biogeochemical zonations in the subterranean estuary. While the pH in the system was relatively stable over the monitoring period, the DO behaved similarly to the salinity in the upper saline plume. These zonations signify the complexity of the geochemical processes in the subterranean estuary and are expected to have important implications for the distribution and fate of reactive chemicals in the system.

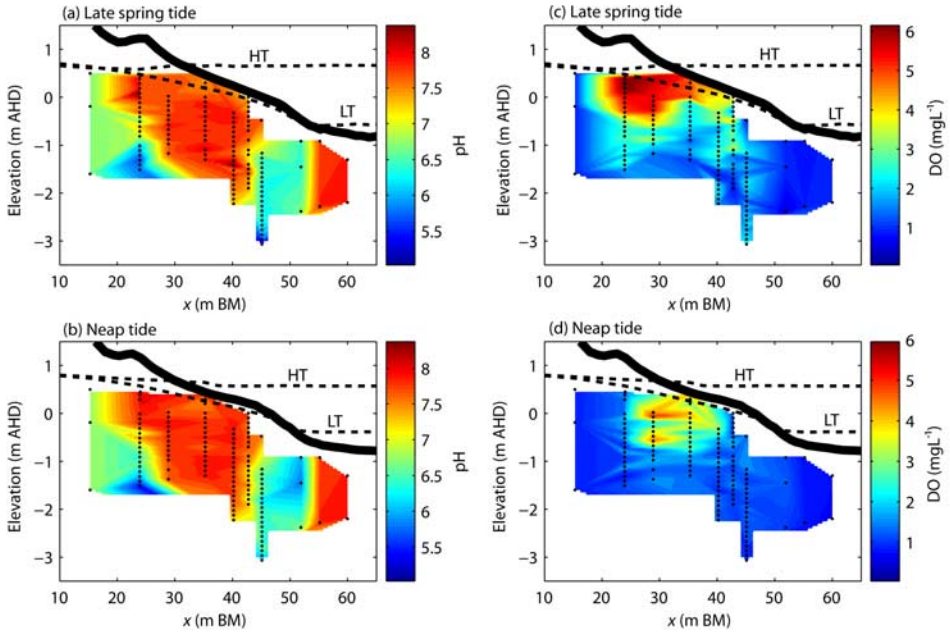


**Figure 17.** Spatial pH distributions measured on (a) 4 elapsed days and (b) 8 elapsed days, and DO distributions measured on (c) 4 elapsed days and (d) 8 elapsed days. Sand levels (—) and maximum high tide (HT) and low tide (LT) water levels recorded (– –) for each day are also shown.

[42] Most previous field studies of flow and transport processes in coastal aquifers neglect the dynamic nature of the flow, water exchange and salinity structure in the intertidal zone. However, these dynamics may affect significantly the transport, mobility and removal of chemicals in the subterranean estuary and their subsequent discharge to coastal waters [*Charette and Sholkovitz*, 2002; *Slomp and Cappellen*, 2004]. The salt-freshwater dynamics revealed here provide new insight into the complexity, intensity and time-scales of mixing between fresh groundwater and recirculating seawater in the tidally influenced subterranean estuary, and the driving mechanisms for flow and water exchange near and across the aquifer-ocean interface.

[43] **Acknowledgments.** The authors thank those who assisted in the collection of field data including Julia Derx, Mothei Lenkopane, Paul Guard, Matthew Barnes, Mirium El Bettah and Audrey Gertsch. We would also like to thank Peter Nielson, Nick Cartwright, Dave Callaghan and Tom Baldock for their assistance in the development of field methods. We acknowledge the Queensland Parks and Wildlife Service for allowing us to conduct research in Moreton Island National Park (Scientific Purposes Permit: WITK02602804). This study was supported by funding from Australian Research Council (DP0346461) and National Natural Science Foundation of China (50425926). Financial assistance of an Australian Postgraduate Award to the first author is also gratefully acknowledged. Comments from three anonymous reviewers have led to improvement of the paper.

## References

Appelo, C. A. J., and D. Postma (2005), *Geochemistry, groundwater and pollution*, A. A. Balkema Publishers, Leiden, The Netherlands.

Ataie-Ashtiani, B., R. E. Volker, and D. A. Lockington (1999), Tidal effects on sea water intrusion in unconfined aquifers, *J. Hydrol.*, *216*, 17–31.

Barry, D. A., and J. Y. Parlange (2004), Subsurface pathways of contaminants to coastal waters, in *Proceedings of 6th International Conference on Hydroscience and Engineering*, Brisbane, May 30–June 3.

Boehm, A. B., A. Paytan, G. G. Shellenbarger, and K. A. Davis (2006), Composition and flux of groundwater from a California beach aquifer: Implications for nutrient supply to the surf zone, *Cont. Shelf Res.*, *26*(2), 269–282, doi:10.1016/j.csr.2005.11.008.

Boufadel, M. C. (2000), A mechanistic study of nonlinear solute transport in a groundwater-surface water system under steady state and transient hydraulic conditions, *Water Resour. Res.*, *36*(9), 2549–2565.

Burnett, W. C., H. Bokuniewicz, M. Huettel, W. S. Moore, and M. Taniguchi (2003), Groundwater and pore water inputs to the coastal zone, *Biogeochem.*, *66*, 3–33.

Cartwright, N., and P. Nielsen (2001), Groundwater dynamics and salinity in coastal barriers, in *Proceedings of First International Conference on Saltwater Intrusion and Coastal Aquifers - Monitoring, Modeling, and Management*, Essaouira, Morocco, April 23–25.

Cartwright, N., L. Li, and P. Nielsen (2004), Response of salt-freshwater interface in a coastal aquifer to a wave-induced groundwater pulse: Field observations and modelling, *Adv. Water Resour.*, *27*(3), 297–303, doi:10.1016/j.advwatres.2003.12.005.

Charette, M. A., and E. R. Sholkovitz (2002), Oxidative precipitation of groundwater-derived ferrous iron in the subterranean estuary of a coastal bay, *Geophys. Res. Lett.*, *29*(10), 1444, doi:10.1029/2001GL014512.

Charette, M. A., and E. R. Sholkovitz (2006), Trace element cycling in a subterranean estuary: Part 2. Geochemistry of the pore water, *Geochim. Cosmochim. Acta*, *70*, 811–826, doi:10.1016/j.gca.2005.10.019.

Church, T. (1996), An underground route for the water cycle, *Nature*, *380*, 579–580.

Cooper, H. H. (1959), A hypothesis concerning the dynamic balance of fresh water and salt water in a coastal aquifer, *J. Geophys. Res.*, *64*(4), 461–467.

Ghyben, W. B. (1899), Notes in verband met voorgenomen put boring Nabji Amsterdam, Tijdschrift van let koninklijk Institut van Ingeniers, Hague, Netherlands.

Guo, W., and C. D. Langevin (2002), User's Guide to SEAWAT: A Computer Program for Simulation of Three-Dimensional Variable-Density Ground-Water Flow, *Techniques of Water-Resources Investigations 6-A7*, pp. 77, U. S. Geological Survey, Tallahassee, Florida.

Hem, J. D. (1985), *Study and interpretation of chemical characteristics of natural water*, 3rd ed., U. S. Geological Survey, Alexandria, VA.

Herzberg, A. (1901), Die Wasserversorgung einiger Nordseebder, *Zeitshriftfur Gasbeleuchtung und Wasserversorgung*, *44*, 815–819.

Hussain, N., T. M. Church, and G. Kim (1999), Use of $^{222}$Rn and $^{226}$Ra to trace groundwater discharge into Chesapeake Bay, *Mar. Chem.*, *65*, 127–134.

Hvorslev, M. J. (1951), Time lag and soil permeability in ground-water observations, *Bulletin no. 36*, 50 pp., U.S. Army Corps of Eng., Waterways Experiment Station, Mississippi.

Kim, G., and D. W. Hwang (2002), Tidal pumping of groundwater into the coastal ocean revealed from submarine $^{222}$Rn and $CH_4$ monitoring, *Geophys. Res. Lett.*, *29*(14), 1678, doi:10.1029/2002GL015093.

Kim, G., K. K. Lee, K. S. Park, D. W. Hwang, and H. S. Yang (2003), Large submarine groundwater discharge (SGD) from a volcanic island, *Geophys. Res. Lett.*, *30*(21), 2098, doi:10.1029/2003GL018378.

Langevin, C., W. B. Shoemaker, and W. Guo (2003), Modflow-2000, The U. S. Geological Survey modular ground-water model - Documentation of the Seawat-2000 version with the variable density flow process (VDF) and the integrated MT3DMS transport process (IMT), *U.S. Geol. Surv. Open File Rep. 03-426*, pp. 57, Tallahassee, Florida.

Li, L., and D. A. Barry (2000), Wave-induced beach groundwater flow, *Adv. Water Resour.*, *23*, 325–337.

Li, L., D. A. Barry, F. Stagnitti, and J.-Y. Parlange (1999), Submarine groundwater discharge and associated chemical input to a coastal sea, *Water Resour. Res.*, *35*(11), 3252–3259.

Li, L., A. J. Baird, and D. Horn (2002), Spring-neap tidal water table fluctuations in a coastal aquifer: beach slope-seepage face effects, in *Proceeding of ICCE 2002, 28th International Conference on Coastal Engineering*, Cardiff, 7–12 July.

Longuet-Higgins, M. S. (1983), Wave set-up, percolation and undertow in the surf zone, *Proc. R. Soc. Lond., A*, *390*, 283–291.

Mango, A. J., M. W. Schmeeckle, and D. J. Furbish (2004), Tidally induced groundwater circulation in an unconfined coastal aquifer modeled with a Hele-Shaw cell, *Geology*, *32*(3), 233–236.

Mao, X., P. Enot, D. A. Barry, L. Li, A. Binley, and D.-S. Jeng (2006), Tidal influence on behaviour of a coastal aquifer adjacent to a low-relief estuary, *J. Hydrol.*, *327*, 110–127, doi:10.1016/j.jhydrol.2005.11.030.

Martin, J. B., K. M. Hartl, D. R. Corbett, P. W. Swarzenski, and J. E. Cable (2003), A multi-level pore-water sampler for permeable sediments, *J. Sediment. Res.*, *73*(1), 128–132.

McLachlan, A., and I. Turner (1994), The interstitial environment of sandy beaches, *Mar. Ecol.*, *15*(3–4), 177–211.

Michael, H. A., A. E. Mulligan, and C. F. Harvey (2005), Seasonal oscillations in water exchange between aquifers and the coastal ocean, *Nature*, *436*, 1145–1148, doi:10.1038/nature03935.

Miller, D. C., and W. J. Ullman (2004), Ecological consequences of ground water discharge to Delaware Bay, United States, *Ground Water*, *42*(7), 959–970.

Moore, W. S. (1996), Large groundwater inputs to coastal waters revealed by $^{226}$Ra enrichments, *Nature*, *380*, 612–614.

Moore, W. S. (1999), The subterranean estuary: A reaction zone of ground water and sea water, *Mar. Chem.*, *65*, 111–125.

O'Neil, J. M., and W. C. Dennison (2005), Chapter 6: Lyngbya, in *Healthy Waterways Healthy Catchments: Making the connection in South East Queensland, Australia*, edited by E. G. Abal, S. E. Bunn et al., 119-148, Moreton Bay Waterways and Catchments Partnership, Brisbane.

Oostrom, M., J. S. Hayworth, J. H. Dane, and O. Guven (1992), Behaviour of dense phase leachate plumes in homogeneous media, *Water Resour. Res.*, *28*(8), 2123–2134.

Pickens, J. F., J. A. Cherry, G. E. Grisak, W. F. Merritt, and B. A. Risto (1978), A multilevel device for groundwater sampling and piezometric modelling, *Ground Water*, *16*(5), 322–327.

Prieto, C., and G. Destouni (2005), Quantifying hydrological and tidal influences on groundwater discharges to coastal waters, *Water Resour. Res.*, *41*, W12427, doi:10.1029/2004WR003920.

Pugh, D. T. (1987), *Tides, surges and mean sea-level*, John Wiley & Sons, Chichester.

Robinson, M. A., and D. L. Gallagher (1999), A model of groundwater discharge from an unconfined aquifer, *Ground Water*, *37*(1), 80–87.

Robinson, M. A., D. Gallagher, and W. Reay (1998), Field observations of tidal and seasonal variations in groundwater discharge to tidal estuarine surface water, *Ground Water Monit. Rem.*, *18*(1), 83–92.

Robinson, C., B. Gibbes, and L. Li (2006), Driving mechanisms for flow and salt transport in a subterranean estuary, *Geophys. Res. Lett.*, *33*, L03402, doi:10.1029/2005GL025247.

Robinson, C., L. Li, and D. A. Barry (2007), Effect of tidal forcing on a subterranean estuary, *Adv. Water Resour.*, *30*, 851–865, doi:10.1016/j.advwatres.2006.07.006.

Schincariol, R. A. (1998), Dispersive mixing dynamics of dense miscible plumes: Natural perturbation initiation by local-scale heterogeneities, *J. Contam. Hydrol.*, *34*, 247–271.

Schincariol, R. A., and F. W. Schwartz (1990), An experimental investigation of variable density flow and mixing in homogeneous and heterogeneous media, *Water Resour. Res.*, *26*(10), 2317–2329.

Simmons, G. M. (1992), Importance of submarine groundwater discharge (SGWD) and seawater cycling to material flux across the sediment/water interfaces in marine environments, *Mar. Ecol. Prog. Ser.*, *84*, 173–184.

Simmons, C. T., T. R. Fenstemaker, and J. M. Sharpe (2001), Variable-density groundwater flow and solute transport in heterogeneous porous media: Approaches, resolutions and future challenges, *J. Contam. Hydrol.*, *52*, 245–275.

Slomp, C. P., and P. V. Cappellen (2004), Nutrient inputs to the coastal ocean through submarine groundwater discharge: Controls and potential impact, *J. Hydrol.*, *295*, 64–86, doi:10.1016/j.jhydrol.2004.02.018.

Spiteri, C., P. Regnier, C. P. Slomp, and M. A. Charette (2005), pH-Dependent iron oxide precipitation in a subterranean estuary, *J. Geochem. Explor.*, *88*, 399–403, doi:10.1016/j.gexplo.2005.08.084.

Staver, K. W., and R. B. Brinsfield (1996), Seepage of groundwater nitrate from a riparian agroecosystem into the Wye River estuary, *Estuaries*, *19*(2B), 359–370.

Taniguchi, M. (2002), Tidal effects on submarine groundwater discharge into the ocean, *Geophys. Res. Lett.*, *29*(12), 1561, doi:10.1029/2002GL014987.

Taniguchi, M., and H. Iwakawa (2004), Submarine groundwater discharge in Osaka Bay, *Limnology*, *5*, 25–32.

Taniguchi, M., W. C. Burnett, J. E. Cable, and J. V. Turner (2002), Investigation of submarine groundwater discharge, *Hydrol. Process.*, *16*, 2115–2129, doi:10.1002/hyp.1145.

Taniguchi, M., T. Ishitobi, and J. Shimada (2006), Dynamics of submarine groundwater discharge and fresh-seawater interface, *J. Geophys. Res.*, *111*, C01008, doi:10.1029/2005JC002924.

Turner, I. L. (1993a), Beach face permeability, the groundwater effluent zone and intertidal profiles of macro-tidal beaches: a conceptual model, in *Catchments and Coasts of Eastern Australia*, edited by M. Thoms, 88-99, Dep. Geogr., Univ. of Sydney *Monogr. Ser.*, Sydney.

Turner, I. L. (1993b), Water table outcropping on macro-tidal beaches: A simulation model, *Mar. Geol.*, *115*, 227–238.

Turner, I. L., and R. I. Acworth (2004), Field measurements of beachface salinity structure using cross-borehole resistivity imaging, *J. Coast. Res.*, *20*(3), 753–760.

Ullman, W. J., B. Chang, D. C. Miller, and J. A. Madsen (2003), Groundwater mixing, nutrient diagenesis, and discharges across a sandy beachface, Cape Henlopen, Delaware (USA), *Est. Coast. Shelf Sci.*, *57*, 539–552.

Urish, D. W. (2004), Determination of the temporal and spatial distribution of beach face seepage, in *Coastal aquifer management: monitoring, modelling and case studies*, edited by A. H. D. Cheng and D. Ouzar, 143-165, Lewis Publishers, New York.

Vandenbohede, A., and L. Lebbe (2005), Occurrence of salt water above fresh water in dynamic equilibrium in a coastal groundwater flow system near De Panne, Belgium, *Hydrogeology J.*, *14*(4), 462–472, doi:10.1007/s10040-005-0446-5.

Watkinson, A. J., J. M. O'Neil, et al. (2005), Ecophysiology of the marine cyanobacterium, Lyngbya majuscula (Oscillatoriaceae) in Moreton Bay, Australia, *Harmful Algae*, *4*, 697–715, doi:10.1016/j.hal.2004.09.001.

Werner, A. D., and D. A. Lockington (2006), Tidal impacts on riparian salinities near estuaries, *J. Hydrol.*, *328*(3–4), 511–522, doi:10.1016/j.jhydrol.2005.12.011.

Westbrook, S. J., J. L. Rayner, G. B. Davis, T. P. Clement, P. L. Bjerg, and S. J. Fisher (2005), Interaction between shallow groundwater, saline surface water and contaminant discharge at a seasonally and tidally forced estuarine boundary, *J. Hydrol.*, *302*, 255–269, doi:10.1016/j.jhydrol.2004.07.007.

Zipperle, A., and K. Reise (2005), Freshwater springs on intertidal sand flats cause a switch in dominance among polychaete worms, *J. Sea Res.*, *54*(2), 143–150, doi:10.1016/j.seares.2005.01.003.

H. Carey, B. Gibbes, and C. Robinson, Environmental Engineering Division, School of Engineering, The University of Queensland, St. Lucia QLD 4072, Australia. (clare.robinson@epfl.ch)

L. Li, Centre for Eco-Environmental Modelling, Hohai University, Nanjing 210098, China.